Self-assembly of an upconverting nanocomplex and its application to turn-on detection of metalloproteinase-9 in living cells

2016 Nanotechnology 27 405101

(http://iopscience.iop.org/0957-4484/27/40/405101)

IOP Publishing Nanotechnology
Nanotechnology **27** (2016) 405101 (9pp) doi:10.1088/0957-4484/27/40/405101

Self-assembly of an upconverting nanocomplex and its application to turn-on detection of metalloproteinase-9 in living cells

Phuong-Diem Nguyen, Vu Thanh Cong, Changyoon Baek and Junhong Min

School of Integrative Engineering, Chung-Ang University, Heukseok-dong, Dongjak-gu, Seoul 156-756, Korea

E-mail: junmin@cau.ac.kr

Received 7 April 2016, revised 15 July 2016
Accepted for publication 20 July 2016
Published 31 August 2016

Abstract

Upcoversion nanoparticles are an emerging luminescent nanomaterial with excellent photophysical properties that have great benefits in biological sensing. In this study, a luminescent turn-on biosensor for cell-secreted protease activity assay is established based on resonance energy transfer in an upconversion nanoparticle–graphene oxide nano-assembly. The proposed biosensor consists of a blue-emitting upconversion nanoparticle covered with a quenching complex, comprising gelatin as the proteinase substrate and graphene oxide nanosheets as luminescence acceptors. After enzymatic digestion, the upconversion nanoparticles lose the gelatin cover due to the disassembly of the quenching complex, thus the upconverting luminescence in the blue region is restored (a turn-on response). The recovered upconverting luminescence is proportional to the protease concentration; the limit of detection was 12 ng ml^{-1}. Finally, the upconversion–graphene oxide nanocomplex was successfully applied in the detection of cell-secreted protease-metalloproteinase in MCF-7 cancer cells with high sensitivity and specificity.

S Online supplementary data available from stacks.iop.org/NANO/27/405101/mmedia

Keywords: upconversion nanoparticle, resonance energy transfer, graphene oxide nanosheets, quenching, metalloproteinase

(Some figures may appear in colour only in the online journal)

1. Introduction

The matrix metalloproteinases (MMPs) are a group of proteases that are up-regulated in almost every type of human cancer cell line [1]. An increased amount of MMP-9, a member of the MMP family, has been reported in samples taken from rats and humans with malignant tumors [2, 3]. Therefore, MMPs has been extensively studied as an important biomarker for cancer diagnosis. Substrate zymmography was the first approach for MMP detection, however, this method is very time-consuming and exhibits low sensitivity [4]. Other standard assays for MMP activity include those based on enzyme-linked immunosorbent assays, chemoluminescence, radioisotopes, or Foster resonance energy transfer (FRET)-based sensors [5–7]. FRET is one of the most attractive methods for MMP-9 detection, based on its simple fabrication and high sensitivity. The standard configuration of a FRET-based sensor generally includes organic fluorophores or quantum dots (QDs) as energy donors. Although there are many strategies for the design of FRET sensors, the detection sensitivity is determined by fluorophores. Organic fluorophores suffer from

photobleaching, while QD material suffers from blinking effects. However, the main disadvantage results from the excitation wavelength of these materials, which are mainly located in the ultraviolet (UV)–vis region. In this region, the fluorescent background coming from the biomolecules and the near inner filter effect provoked by other species can dramatically decrease the detection sensitivity [8, 9]. Therefore, there is a crucial need to develop an alternative for conventional UV-excited fluoroprobes in FRET-based bioassays.

Upconversion nanoparticles (UCNP) doped with rare-earth ions are a new class of materials that have attracted increasing interest due to their unique optical properties compared to conventional fluorescent materials. In contrast to UV-excited fluorophores, UCNPs emit high-energy photons under low-energy excitation (near-infrared (NIR), typically 980 nm), resulting in a non-linear optical upconversion process [10]. Because two or more photons are required in the upconversion process, it violates the Stoke shift rules (so-called anti-Stoke shift), resulting in the emission spectra occurring at a shorter wavelength (the visible region) [11]. In comparison to fluorophores and QDs, UCNPs exhibit outstanding luminescence intensity, high photostability, low cytotoxicity, and sharp anti-Stoke shift emission spectra. Moreover, their unique NIR-excitation nature can overcome the autofluorescent background from biological samples, which is beneficial for the detection of biomolecules [10–12]. When utilizing UCNPs as luminescent reporters in a FRET sensor, the superior upconverting properties can overcome most, if not all, the deficiencies of conventional UV-excited materials shown in bioassays.

Based on the considerations above, we strategically designed a luminescent-RET (LRET) system using UCNP and graphene oxide (GO) as the energy donor–acceptor pair for *in vitro* detection of MMP-9, an important biomarker for cancer metastasis and tumor progression [13–15]. Gelatin B, a biocompatible and non-immunogenic substrate for MMP-9 activity, was employed in the LRET system, not only as an enzyme responsive linker but also as a stabilizing agent against GO agglomeration [16–18]. In combination with the high photoluminescence of UCNPs and the strong quenching ability of GO, the developed UCNP–gelatin–GO (UCNP@gel@GO) nanocomplexes were able to selectively and specifically detect MMP-9 in cancer cells by the turn-on response of the UCNPs (figure 1). In comparison to conventional zymography and the enzyme-link immunosorbent assay (ELISA) method, in terms of time and processes (zymography: 18 h, 3 steps; ELISA: 5 h, 9 steps), our UCNP-based sensor shows dramatic improvement (2 h, 1 step). To the best of our knowledge, our study is the first report on UCNP application for quantifying secreted MMP-9 in living cancer cells. Our method could be highly significant for early-stage diagnosis and related biological research, such as bioimaging-guided therapy.

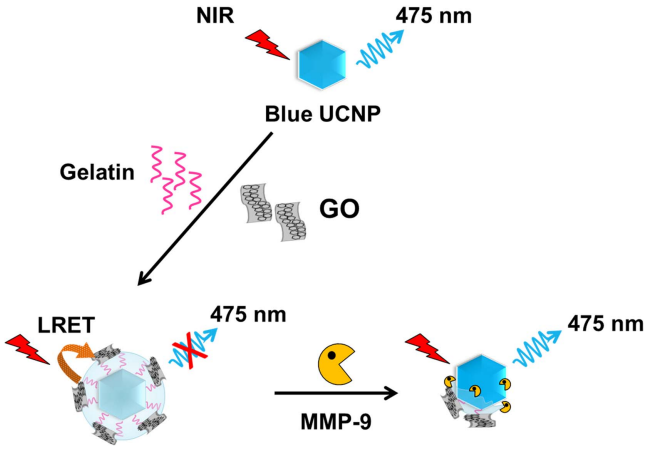

Figure 1. Schematic diagram of MMP-9 detection by a UCNP LRET-based biosensor in the turn-on response manner.

2. Materials and methods

2.1. Preparation of silica coated UCNPs

The UCNPs were fabricated using the co-precipitation method [19–23]. In short, a methanolic solution of YCl_3 (2 ml, 0.4 M), $YbCl_3$ (0.45 ml, 0.4 M), and $TmCl_3$ (0.05 ml, 0.4 M) was added to a three-neck flask containing 6 ml of oleic acid and 1-octadecene. The mixture was heated to 140 °C to obtain a clear solution. After cooling to room temperature, 10 ml methanolic solution of ammonium fluoride (0.15 g) and sodium hydroxide (0.1 g) was added drop-wise under stirring. The mixture was heated to 110 °C to evaporate the methanol and water, and then the temperature was increased to 300 °C under nitrogen protection for 1 h in order to grow the nanoparticles. After cooling, the UCNPs were purified and stored in toluene.

Silica coated UCNPs were prepared using the reverse microemulsion method [24]. The microemulsion solution was prepared from cyclohexane (5 ml), poly(oxyethylene) nonylphenyl ether (400 μl) (known as Igepal CO-520), and UCNP (10 mg). The mixture was sonicated for 30 min. Ammonium water (40 μl) was then quickly added and the solution was vigorously stirred. Tetraethyl orthosilicate (10 μl) was subsequently added and the solution was reacted at room temperature for 4 h. The silica coated UCNPs were then washed with ethanol and finally stored in distilled water before use.

2.2. Preparation of the gelatin–GO nanocomplex coated UCNPs (UCNP@gel@GO)

A modified desolvation method was employed to purify the gelatin prior to synthesis. Gelatin type B (0.625 g) was dissolved in 12.5 ml of deionized (DI) water at 40 ± 1 °C. Acetone (12.5 ml) was added to the solution at the rate of 6 ml min^{-1}. Exactly 1 min after acetone addition was complete, the supernatant containing low molecular weight gelatin was removed, and DI water (12.5 ml) was added to the remaining precipitate and heated again at 40 ± 1 °C with constant

stirring. The purified gelatin was lyophized and stored at 4 °C for later use.

To prepare the gelatin–GO quenching complex coated UCNPs (UCNP@gel@GO), GO nanosheets (1 mg, 5 ml, Sigma) were carboxylated by mixing with NaOH (5 g) and trichloroacetic acid (5 g), and sonicated for 2 h. The collected GO was then washed with distilled water repeatedly by centrifugation at 13 000 rpm until a well-dispersed GO suspension was obtained. The GO suspension was then treated with an ultrasonication probe at 250 W for 1 h in order to break the GO sheets into proper sizes for nanoparticle wrapping. The resultant GO–COOH broken sheets were then added into 1% gelatin solution and the mixture was stirred for 2 h at 50 ± 1 °C until a homogeneous solution was obtained. UCNPs (5 mg) were subsequently added and the resultant mixture was stirred for an additional 4 h at 50 ± 1 °C to complete the noncovalent adsorption process. Then 5 ml of cold DI water was quickly added, followed by the injection of 2.5 μl of glutaraldehyde solution (25%) to initiate the crosslinking of the gelatin. The solution was stirred for an additional hour, then the obtained nanocomplex was collected by centrifugation at 8000 rpm and washed with DI water. The final product was stored in Tris–HCl buffer at 4 °C.

2.3. Detection of MMP-9

Latent pro-MMP-9 was activated using 4-aminophenyl mercuric acetate (APMA; 1 mM) using Tris–HCl buffer (50 mM, pH 7.6) at 37 °C for 4 h, in accordance with the manufacturer's instructions (Sigma, USA). Then UCNP@gel@GO (300 μg) was added into gradient concentrations of activated MMP-9 (0, 6.5, 12.5, 25, 37.5, 50, 75, 100, 125 ng) in Tris–HCl buffer (50 mM, pH 7.6). The reaction mixture was incubated for 3 h at 37 °C with gentle shaking and the luminescence response was measured under 980 nm excitation. The recovery of UCNP luminescence intensity was calculated by the following equation:

$$\text{recovery of luminesccence (RL)} = \frac{I}{I_o}$$

where I is the recovered (dequenched) luminescence intensity of UCNP@gel@GO after incubation with MMP-9, and I_o is the original quenched luminescence intensity. To determine the effect of the inhibitor, the tissue inhibitor of MMP-9 (TIMP; 200 μM) was pre-incubated with MMP-9 for 30 min at 37 °C, then UCNP@gel@GO was added and the mixture was reacted for 2 h at 37 °C.

2.4. Detection of MMP-9 secreted from living cells

MCF-7 cells were seeded in 10 cm dishes at a density of 2.5×10^4 cells per dish and cultured in RPMI containing 10% fetal bovine serum and 1% penicillin-streptomycin until the cell confluence reached 60%. A solution of phorbol myristate acetate (PMA; 0.2 μM final concentration) in RPMI media was added and the cells were incubated for specific time intervals (i.e. 4, 8, 12 h). Then the conditioned cell-cultured media were taken out to be mixed with UCNP@gel@GO (300 μg ml^{-1}). The luminescence response of the nanosensor was measured using a Spectra Suit spectrophotometer under a 980 nm continuous laser.

The concentrations of MMP-9 secreted from living cells were further determined by the gold standard MMP-9 human ELISA kit (Sigma, USA). 100 μl of a solution of standard and conditioned cell-cultured media was added into the human MMP-9 specific antibody coated wells. After 2.5 h incubation at room temperature with gentle shaking, the solution was removed. 100 μl of biotinylated MMP-9 detection antibody was added and incubated for 1 h at room temperature with gentle shaking. The washing step was repeated, and then 100 μl of TMB one-step substrate reagent was added to each well and incubated for 30 min at room temperature in the dark with gentle shaking. Absorbance was measured at 450 nm using a microplate spectrophotometer (Synergy, Biotek Instrument, USA) immediately after adding 50 μl of stop solution.

2.5. Immunofluorescent assay

Filamentous actin (F-actin) and vinculin (a focal adhesion protein) were analyzed using immunofluorescence staining using an Actin Cytoskeleton and Focal Adhesion Staining Kit (Millipore, Darmstadt, Germany) following the manufacturer's protocol. Cultured cells were fixed by 4% paraformaldehyde for 15 min and rinsed three times with 1× phosphate buffered saline (PBS) solution. Blocking solution (1× PBS, 5% horse serum, 0.3% Triton X-100) was added and the mixture was incubated for 30 min at room temperature. The first antibody (250:1) was diluted in antibody solution (1× PBS, 1% BSA, 0.3% Triton X-100) and incubated for 12 h at 4 °C. Next, it was washed three times with 1× PBS solution. The FITC-conjugated secondary antibody (250:1) was diluted in antibody solution and incubated for 2 h at room temperature. The resulting product was rinsed three times with 1× PBS and staining of nuclei was performed by treatment with 4′,6-diamidino-2-phenylindole (DAPI; Sigma-Aldrich) solution for 5 min.

3. Results and discussion

3.1. UCNP@gel@GO nanocomplex characterization

First, the modified bottom-up approach was employed to fabricate blue-emissive upconverting nanocrystals. The host material of the UCNP consists of hexagonal phase $NaYF_4$, which is doped with 25 mol% of Yb^{3+} and 0.3 mol% of Tm^{3+} ions. The successful fabrication of UCNPs was characterized by transmission electron microscopy (TEM), optical NIR excitation at 980 nm, dynamic light scattering (DLS), and energy-dispersive x-ray spectroscopy (EDS). Figures 2(A) and (B), respectively, show a TEM image and the blue emission of the synthesized upconversion nanocrystals. Figure 2(C) shows the luminescence spectral

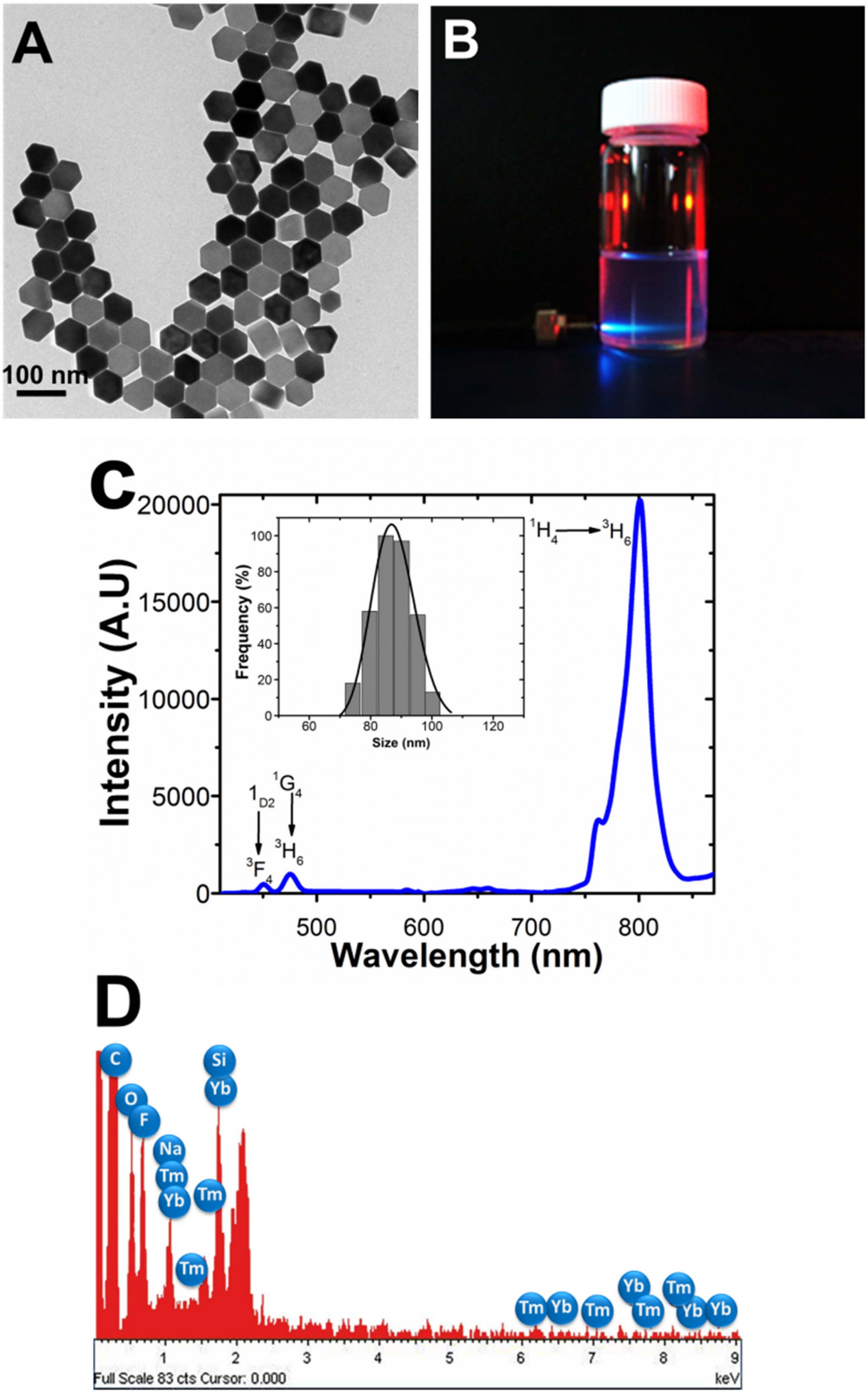

Figure 2. Characterization of the as-synthesized UCNPs. (A) TEM image of UCNPs. (B) Blue-emitting UCNPs under 980 nm excitation. (C) UCNP luminescence spectrum under 980 nm excitation; the inset shows the DLS size distribution. (D) EDS spectrum of silica coated UCNPs.

graph which displays three upconversion maxima in total, the highest one in NIR 800 nm and the two smaller ones at ~475 and ~485 nm, respectively. According to the characterization data, the nanoparticles possess a hydrodynamic size of roughly 80 nm with a distinctive hexagonal structure and upconverting emission at the blue region. The EDS results showed the signals of seven elements, Na, F, Y, Yb, Tm, Si, and O, in the composition of the silica coated UCNPs (figure 2(D)). The silica coated UCNPs were well dispersed in the water and buffer solution.

Gelatin capping onto silica coated UCNPs was performed via temperature induced gelation and glutaraldehyde mediated crosslinking. The gelatin coating and GO assembly on UCNPs (UCNP@gel@GO nanocomplex) were characterized by DLS, TEM, Fourier transform infrared spectroscopy (FTIR), and UV–vis absorbance. Figure 3(A) shows the DLS results for the formation of the UCNP@gel@GO nanocomplexes, in which the average size of the UCNPs increased from 80 nm to roughly 150 nm, indicating the coordination of the gelatin–GO quencher complex. To directly observe the morphological change of the UCNPs during synthesis, TEM was used (figure 3(A), inset). According to the TEM results, the hexagonal UCNP was imbedded inside a homogeneous gelatin–GO layer. GO sheets were attached onto the surface of UCNP@gel forming bulky agglomerates with a layered structure at the edges. TEM imaging was the most direct evidence to prove the successful coating of gelatin and GO sheets around UCNPs. The formation of the nanocomplex was further investigated by FTIR (figure 3(B)) and UV–vis spectroscopy (figure 3(C)). The gelatin spectrum was characterized by a large band around 3450 cm^{-1}, corresponding to N–H stretching vibration, two narrow bands at 2920 and 2850 cm^{-1} attributed to C–H_2 stretching vibration, bands between 1750 and 150 cm^{-1} corresponding to amide vibrations, and a narrow peak at 1400 cm^{-1} indicating the presence of the carboxylate group [25]. The silica coated UCNP spectrum showed an intense band in the range of 1100–900 cm^{-1}, which corresponds to the vibration of the Si–O or Si–O–Si group. In the UCNP@gel spectrum, this characteristic band of the silanol group was observed to have significant attenuation, which was presumably caused by the coordination of gelatin. More importantly, the UCNP@gel@GO spectrum shows a characteristic absorption band at 1544 cm^{-1} associated with the stretching vibration of N–H bending of gelatin, while the silica coated UCNPs had no adsorption at that wavelength, confirming the coordination of gelatin on the UCNP surface. A reduction in the peak intensity is anticipated as a result of the combined effects of conformational change in the protein chain of the gelatin and the interaction between the gelatin molecule and silanol hydrogen. A similar phenomenon also appeared in a previous work [26]. Figure 3(C) shows the optical properties of UCNP@gel@GO characterized by UV–Vis spectroscopy. After gelatin coating, the spectrum of UCNP@gel (red dotted line) shows the characteristic peak at about 266 nm which is assigned to gelatin. After subsequent GO coating, the peak at 300 nm, due to n–p^* transitions of C=O, C–O–C, and O–O bonds on GO, were found in the spectrum of the

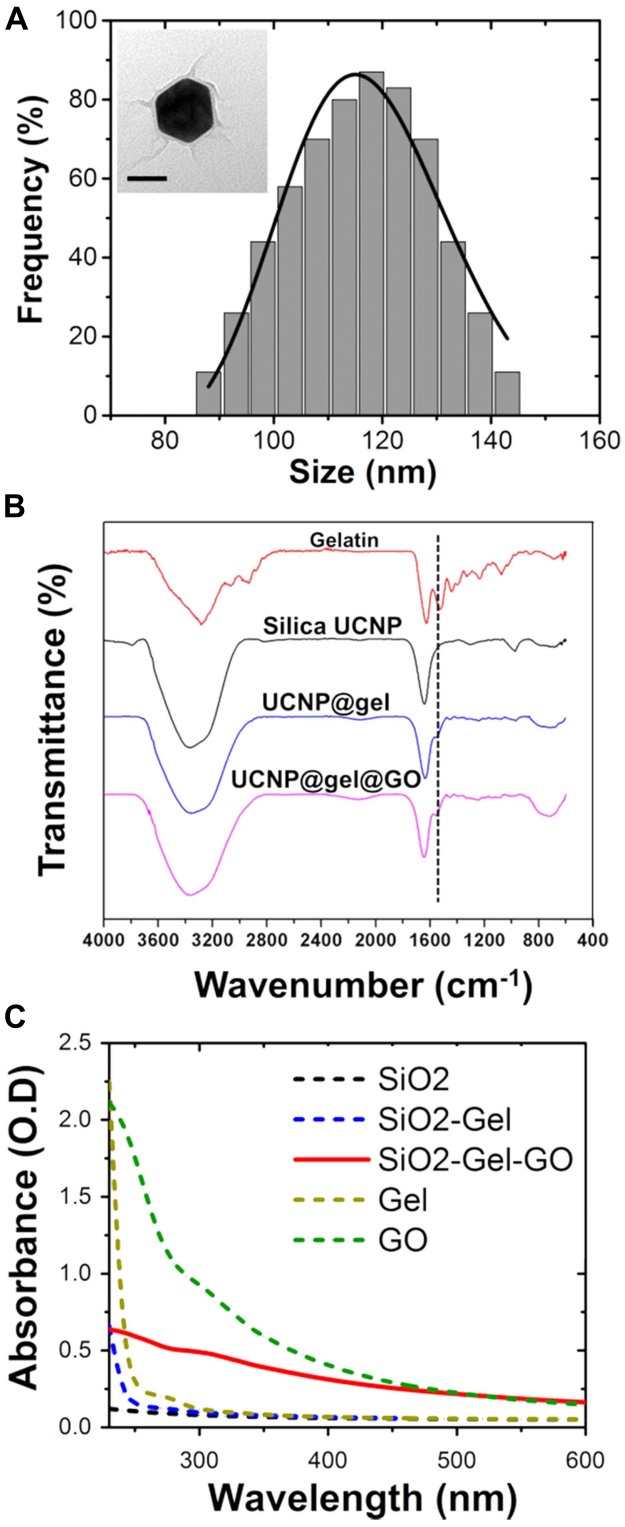

Figure 3. Characterization of the UCNP@gel@GO nanocomplex. (A) DLS size distribution; the inset shows a TEM image of the nanocomplex, scale bar 100 nm. (B) FTIR results. (C) UV–vis adsorption of gelatin, silica coated UCNP, UCNP@gel, and the UCNP@gel@GO nanocomplex.

UCNP@gel@GO solution, proving the successful coating of GO on UCNPs [27]. The UCNP@Gel@GO nanocomplexes are readily dispersed in water and buffer solution under just mild ultrasonic treatment.

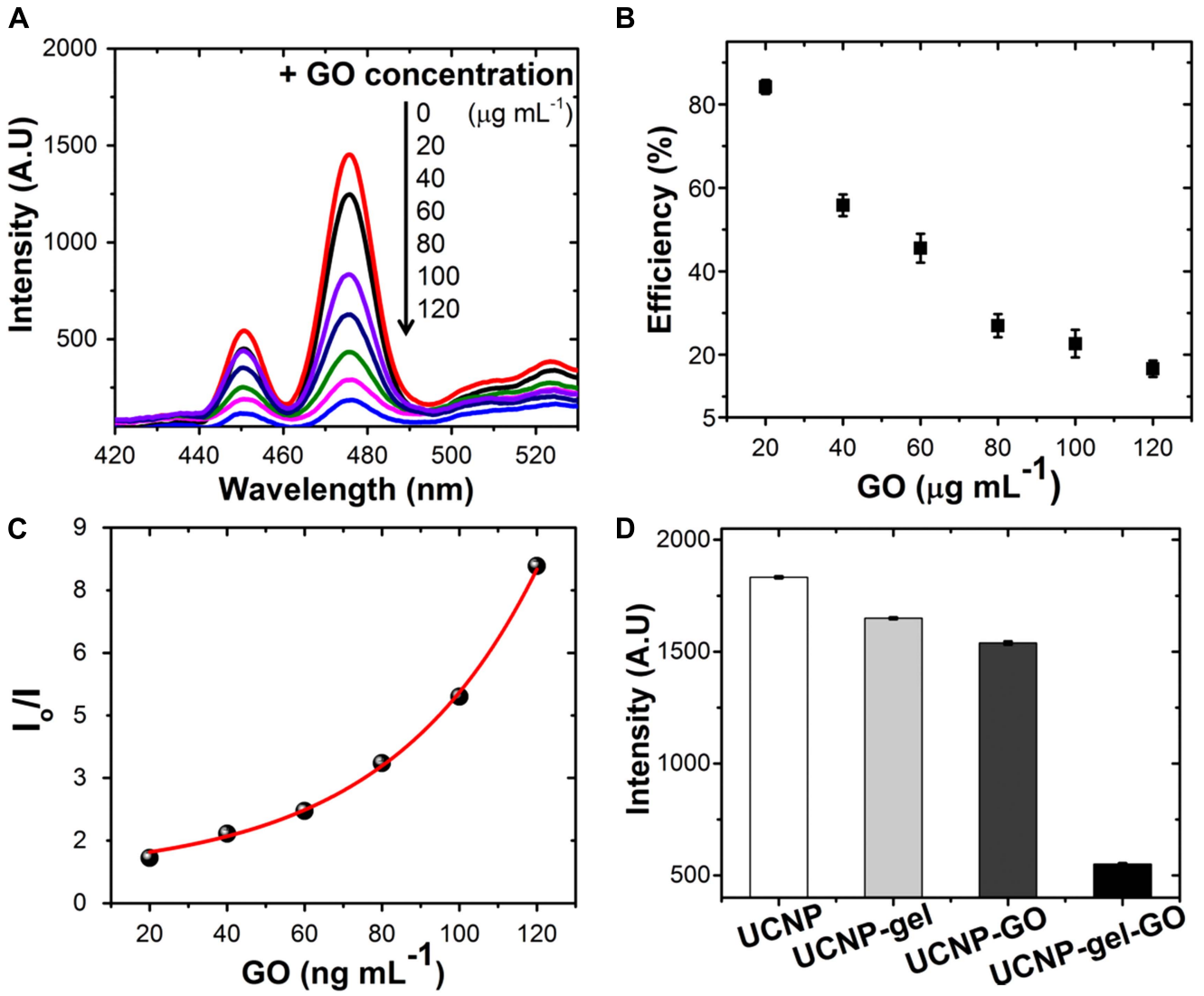

Figure 4. The effects of GO quenching on UCNP luminescence intensity. (A) The decrease of UCNP intensity upon addition of GO. (B) The quenching efficiency of different GO concentrations against UCNP intensity. (C) Stern–Volmer plot of UCNP intensity before (I_o) and after (I) GO addition. (D) GO quenching against UCNP intensity in the absence and presence of gelatin.

3.2. UCNP quenching mechanism

According to the spectra, the blue upconverting emissions have a large spectral overlap with the absorption spectrum of GO (black curve, figure S1 in online supporting information) and thus will be useful in a LRET system [28]. The GO quenching effect was investigated by adding increasing GO concentrations to the gelatin coated UCNPs. As is shown in figure 4(A), the addition of GO solution induced an instantaneous decrease in UCNP intensity. The influence of the GO concentration on quenching efficiency at 475 nm is shown in figure 4(B). In a comparison of the emission spectra of UCNPs with and without GO coating, a remarkable quenching (~88%) was obtained when 120 μg GO was added. Quenching efficiency increased when the GO concentration increased from 20–120 μg ml^{-1}. Figure 4(C) shows the characteristic upward curvature of the Stern–Volmer equation by plotting the UCNP intensity ratio before (I_o) and after (I) adding GO (I_o/I). According to the literature [29, 30], a Stern–Volmer upward curvature plot is thought to show the presence of static quenching due to the formation of dark complexes (quenched fluorescence). The quenching rate constant was calculated to be 35 $\times$ 10^3 (μg ml^{-1})$^{-1}$.

With the aim of assessing the importance of gelatin for the interaction between UCNP and GO, we compared the intensity of UCNP–GO with and without the presence of intercalating gelatin. As expected, simple physical mixing of UCNPs and GO without adding gelatin showed insignificant quenching (figure 4(D), dark gray bar). The results indicate that gelatin plays an important role in UCNP quenching phenomena. It is suggested that gelatin induces the quenching by reducing the proximity between the UCNPs and GO in solution, thus facilitating LRET. The simple nonspecific absorption process of GO on UCNPs was insignificant in our experimental conditions. Although the luminescence intensity was quenched by 88% when the GO concentration reach 120 μg, a high GO concentration was observed to decrease the

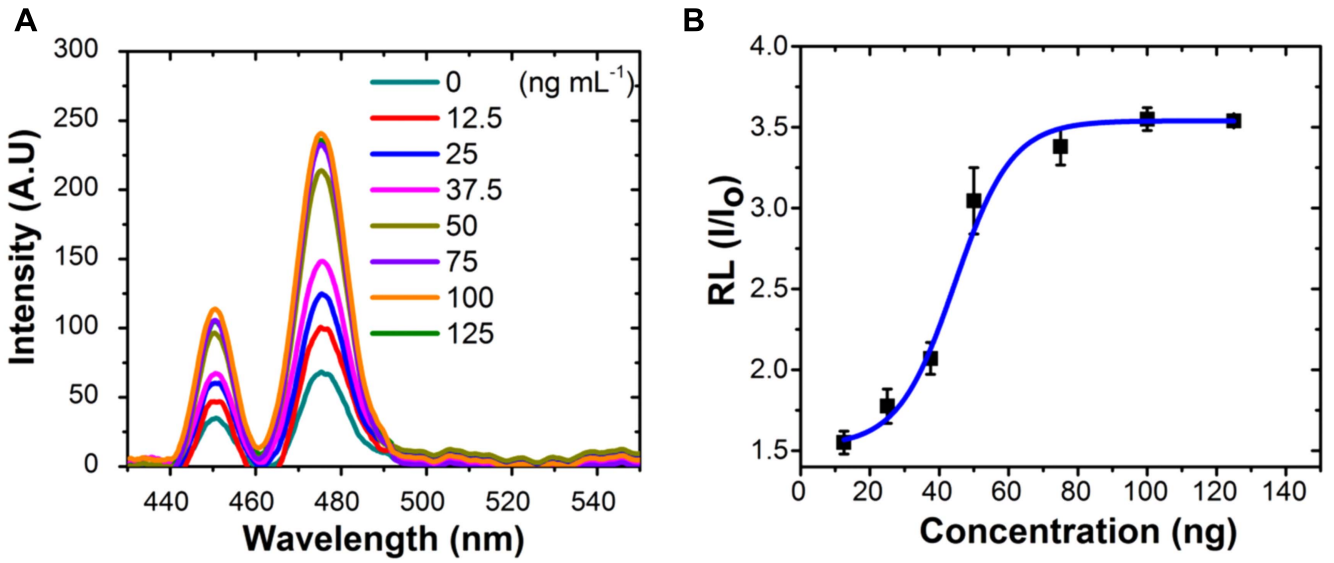

Figure 5. UCNP@gel@GO nanocomplex under MMP-9 challenge. (A) UCNP recovered intensity upon MMP-9 addition. (B) Recovered luminescence (RL; I/I_o, I_o, and I are the quenched- and dequenched luminescence, respectively).

sensitivity of the assay (data not shown). Therefore, a 90 μg GO concentration was selected as the optimum concentration for quenching 5 mg of UCNPs.

3.3. Application of the UCNP@gel@GO nanocomplex for MMP-9 detection

To investigate the stability of the UCNP@gel@GO nanocomplex under 980 nm excitation, a pre-determined amount of the nanocomplex was irradiated under a continuous 980 nm light source for 30 min and the resulting nonspecific upconversion intensity was recorded. Figure S2 in the supporting information shows the recovery luminescence after different exposure time. The results show that there was almost no significant increase in UCNP intensity after 30 min of continuous exposure, implying the stability of the nanocomplex under NIR irradiation.

The capability of the as-prepared nanocomplex in MMP-9 detection was evaluated by challenging the nanocomplex with increasing enzyme concentrations. Proenzyme MMP-9, after activation with APMA, was added to UCNP@gel@GO and was incubated at 37 °C with gentle shaking. Then the resulting solution was irradiated under 980 nm excitation and the UCNP intensity was recorded. The recovery of luminescence intensity was calculated based on the UCNP intensity before (I_o) and after (I) adding MMP-9 (I/I_o). It was observed that the quenched luminescence of the nanocomplex was restored after the addition of MMP-9 and the luminescence recovery increased with increasing enzyme concentration (figure 5(A)). The most linearity was obtained at an enzyme concentration from 12.5 to 80 ng ml^{-1}, and saturation was obtained at 120 ng ml^{-1}(figure 5(B)). The luminescence responses were very stable and no luminescence recovery was observed in the control experiment, where UCNP@gel@GO was incubated in the absence of the enzyme. Figure S3 in the supporting information shows a TEM image of the UCNP@gel@GO nanocomplex after enzyme challenge, the inset clearly shows the digested gel@GO quencher complex from the UCNP surface. The results show that the UCNP@gel@GO nanocomplex was able to detect the MMP-9 tumor biomarker through a turn-on response of the quenched UCNP.

3.4. Application of the UCNP@gel@GO nanocomplex for MMP-9 detection in living cells

MMP-9 detection is important for the clinical diagnosis and treatment of cancers at an early stage. Therefore, the UCNP@gel@GO nanocomplex was applied for the detection of MMP-9 secreted from MCF-7 cells under the stimulation of PMA. PMA is known to strongly stimulate cancer cell invasion and migration by inducing overexpression of MMP-9 [31, 32]. Immunofluorescence images (figures 6(A), (B)) show the morphological changes during the cell adhesion and spreading processes. After 12 h, the PMA-treated cells (figure 6(B)) were observed to express a remarkable enhancement in colony-forming ability, in particular a condensed distribution of F-actin (red) protruding at the cell edges in comparison to untreated cells (figure 6(A)). These results are consistent with previous reports on MCF-7 morphological changes due to MMP-9 overexpression under PMA stimulation [33, 34].

To confirm the sensitivity of MMP-9 detection using the UCNP@gel@GO nanocomplex, the amount of cell-secreted MMP-9 was determined using both the UCNP@gel@GO nanocomplex and the gold standard ELISA assay (figure 6(C)). It is clearly shown in figure 6(C) that the amount of human MMP-9 secreted from MCF-7 cells increased as a function of cell culture time. The quenched upconversion luminescence was gradually restored with increasing cell incubation time (figure 6(C), blue line). After 12 h of cell incubation with PMA, 19 ng ml^{-1} of MMP-9 was

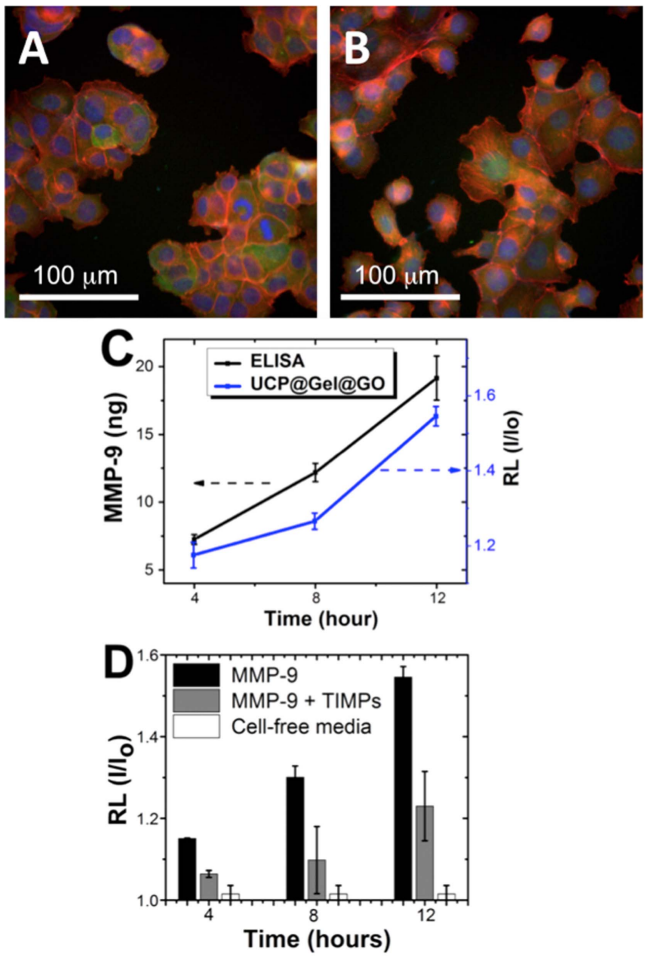

Figure 6. The sensitivity and selectivity of the UCNP@gel@GO nanocomplex for MMP-9 detection in living MCF-7 cells. Immunofluorescence images (red: F-actin; green: vinculin; blue: nucleus) of MCF-7 cells in (A) the absence of PMA and (B) the presence of PMA. (C) Turn-on luminescence response of the UCNP@gel@GO nanocomplex (blue line) and ELISA (black line) for *in vitro* detection of MMP-9 secreted from MCF-7 cells as a function of cell culture time (4 h, 8 h and 12 h). (D) Turn-on luminescence response of the UCNP@gel@GO nanocomplex to cell-secreted MMP-9 in the absence (black bar) and in the presence (gray bar) of TIMP, and the luminescence response of the UCNP@gel@GO nanocomplex in a cell-free medium (white bar).

secreted by MCF-7 cells. The recovery efficiency of the UCNP@gel@GO nanocomplex based assay was 89.67%. The turn-on response of the UCNP luminescence correlated well with the concentration of MMP-9 measured by ELISA, the detection limit was 12 ng ml^{-1}, which is lower than previous nanoparticle-based enzyme sensors [33, 35]. The luminescence response was very stable, and no background fluorescence from the cell medium was recorded under 980 nm excitation, implying the great advantages of UCNP luminescence in bioassays, in particular in complex samples. To confirm that this turn-on response was caused by MMP-9 secreted from the cells, the conditioned cell-cultured media was pre-incubated with 500 μM of MMP-9 inhibitor (TIMP) for 1 h prior to the addition of the UCNP@gel@GO nanosensor. As shown in figure 6(D), a substantial decrease in UCNP turn-on response was observed when MMP-9 activity was inhibited (gray bar), which verifies that the response is caused by MMP-9 secreted from MCF-7 cells only. The obtained results demonstrate that the UCNP@gel@GO nanocomplex can be used for turn-on detection of secreted MMP-9 in living cells with high sensitivity and selectivity.

4. Conclusion

In the present study, a novel LRET-based biosensor using UCNPs as luminescent reporters was synthesized for the quantification of protease biomarker MMP-9 in living cells with high sensitivity. Compared to other commonly used fluorescent materials, the presented biosensor showed excellent stability in different physiological environments, in terms of pH, temperature, and autofluorescent background. Correspondingly, the newly developed sensor was successfully applied for the detection of MMP-9 secreted by the living adenocarcinoma cell line MCF-7 with high sensitivity and satisfactory accuracy (recovery efficiency 89.67%). Furthermore, the proposed nanosensor showed high selectivity in the presence of TIMP; the limit of detection was achieved at 12 ng ml^{-1} and the detection time was significantly reduced compared to the conventional zymography technique (3 h versus 16 h) [36]. To the best of our knowledge, this is the first report demonstrating the application of the UCNP@gel@GO nanosensor for MMP-9 detection *in vitro*. Owing to the novel properties of UCNPs in biological applications, we believe that our proposed nanosensor will significantly contribute to broaden the increasing interest in upconversion based biosensing research and the development of early-stage detection bioassays.

Acknowledgments

This research was supported by the National Research Foundation of Korea (NRF) grant funded by the Korea government (MSIP) (NRF-2016R1A2B4014541).

References

[1] Egeblad M and Werb Z 2002 *Nat. Rev. Cancer* **2** 161–174
[2] Vasala K and Hujanen T T 2007 *Clin. Biochem.* **40** 640–4
[3] Wu Z S, Wu Q, Yang J H, Wang H Q, Ding X D, Yang F and Xu X C 2008 *Int. J. Cancer* **122** 2050–6
[4] Frankowski H, Gu Y, Heo J H, Milner R and del Zoppo G J 2012 *Methods Mol. Biol.* **814** 221–33
[5] Kjeldsen L, Bjerru O W, Hovgaard D, Johnsen A H, Sehested M and Borregaard N 1992 *Eur. J. Haematol.* **49** 180–91
[6] Richard J A, Jean L, Romieu A, Massonneau M, Noack-Fraissigners P and Renard P Y 2007 *Org. Lett.* **9** 4853–5
[7] Edgington L E, Berger A B, Blum G, Albrow V E, Paulick M G, Lineberry N and Bogyo M 2009 *Nat. Med.* **15** 967–73

[8] Chen Z, Chen H, Hu H, Yu M, Li F, Zhang Q, Zhou Z, Yi T and Huang C 2008 *J. Am. Chem. Soc.* **130** 3023–29
[9] Frangioni J V 2003 *Curr. Opin. Chem. Biol.* **2003** 626–34
[10] Helmchen F and Denk W 2005 *Nat. Methods* **2** 932–40
[11] Auzel F 2004 *Chem. Rev.* **104** 139
[12] Suyver J F, Aebischer A, Biner D, Gerner P, Grimm J, Heer S, Kramer K W, Reinhard C and Gudel H U 2005 *Opt. Mater.* **27** 1111
[13] Bérubé M, Deschambeault A, Boucher M, Germain L, Petitclerc E and Guérin S L 2005 *Mol. Vis.* **11** 1101–11
[14] Sato T, Sakai T, Noguchi Y, Takta M, Hirakawa S and Ito A 2004 *Gynecol. Oncol.* **92** 47–56
[15] Di Nezza L A, Misajon A, Zhang J, Jobling T, Quinn M A, Ostör A G, Nie G, Lopata A and Salamonsen L A 2002 *Cancer* **94** 1466
[16] Schyrr B, Boder-Pasche S, Ischer R, Smajda R and Voirin G 2015 *Sens. Bio-Sens. Res.* **3** 65
[17] Veis A (ed) 1964 *The Macromolecular Chemistry of Gelatin* 1st edn (New York: Academic)
[18] Chuang Y, Li Y, Chen S, Liu T, Kuo C, Huang W and Lin C 2010 *Biomaterials* **31** 6087
[19] Hwang S H, Im S G, Sung H, Hah S S, Vu T C, Lee D H, Son S J and Oh H B 2014 *Biosens. Bioelectron.* **53** 112
[20] Wang F, Deng R and Liu X 2014 *Nat. Protoc.* **9** 1634–44
[21] Wang F, Wang J and Liu X 2010 *Angew. Chem. Int. Ed.* **49** 7456–60
[22] Li Z and Zhang Y 2008 *Nanotechnology* **19** 345606
[23] Ryu J, Park H, Kim K, Kim H, Yoo J, Kang M, Im K, Grailhe R and Song R 2010 *J. Phys. Chem.* C **114** 21077–82
[24] Cao X, Li Y, Zhang Z, Yu J, Qian J and Liu S 2012 *Analyst* **137** 5785–91
[25] Gaihre B, Khil M S, Lee D R and Kim H Y 2009 *Int. J. Pharmaceutics* **365** 180
[26] Frydrych M, Wan C, Stengler R, O'Kelly U K and Chen B J 2011 *Mater. Chem.* **21** 9103
[27] Zhu Y W, Murali S, Cai W W, Li X S, Suk J W, Potts J R and Ruoff R S 2010 *Adv. Mater.* **22** 3906
[28] Alonso-Cristobal P, Vilela P, El-Sagheer A, Lopez-Cabarcos E, Brown T, Muskens O L, Rubio-Retama J and Kanaras A G 2015 *ACS Appl. Mater. Interfaces* **7** 12422
[29] Somogyi B, Nyitrai M and Hild G 2007 *Methods in Protein Structure and Stability Analysis: Luminescence Spectroscopy and Circular Dichroism* ed V N Uversky and E A Permyakov (Hauppauge, NY: Nova Science) pp 153–85
[30] Lakowicz J R (ed) 2013 *Principle of Fluorescent Spectroscopy* 2nd edn (New York: Springer Science)
[31] Rucci N, Sanita P and Angelucci A 2011 *Curr. Mol. Med.* **11** 609
[32] Kang H, Jang S W, Park J H and Shim S 2015 *Mol Cell Biochem.* **403** 85–94
[33] Chuang M, Lin S, Chen F, Chu C and Hsu C 2014 *Nanoscale* **6** 1573
[34] Vargová V, Pytliak M and Mechirová V 2012 *EXS.* **103** 1–33
[35] Li J, Lu C H, Yao Q H, Zhang X L, Liu J J, Yang H H and Chen G N 2011 *Biosens. Bioelectron.* **26** 3894
[36] Roomi M W, Monterrey J C, Kalinovsky T, Rath M and Niedzwiecki A 2009 *Oncol. Rep.* **21** 1323–33